https://doi.org/10.5194/acp-2022-294
Preprint. Discussion started: 25 April 2022

Atmospheric Chemistry and Physics Discussions

Effects of OH radical and SO_2 concentrations on photochemical reactions of mixed anthropogenic organic gases

Junling Li[1], Kun Li[2,3], Hao Zhang[1], Xin Zhang[1], Yuanyuan Ji[1], Wanghui Chu[1], Yuxue Kong[1], Yangxi Chu[1], Yanqin Ren[1], Yujie Zhang[1], Haijie Zhang[1], Rui Gao[1], Zhenhai Wu[1], Fang Bi[1], Xuan Chen[1], Xuezhong Wang[1], Weigang Wang[4], Hong Li[1,*], Maofa Ge[4,*]

[1] State Key Laboratory of Environmental Criteria and Risk Assessment, Chinese Research Academy of Environmental Sciences, Beijing 100012, China
[2] Laboratory of Atmospheric Chemistry, Paul Scherrer Institute, 5232 Villigen, Switzerland
[3] Environment Research Institute, Shandong University, Qingdao 266237, China
[4]State Key Laboratory for Structural Chemistry of Unstable and Stable Species Beijing National Laboratory for Molecular Sciences (BNLMS), CAS Research/Education Center for Excellence in Molecular Sciences, Institute of Chemistry, Chinese Academy of Sciences, Beijing 100190, China

Correspondence to: Hong Li (lihong@craes.org.cn), Maofa Ge (gemaofa@iccas.ac.cn)

Abstract. Vehicle exhaust, as a major source of air pollutants in urban areas, contains a complex mixture of organic vapors including long-chain alkanes and aromatic hydrocarbons. The atmospheric oxidation of vehicle emissions is a highly complex system as the co-existing inorganic gases (e.g., NO_x and SO_2) from other urban sources, and therefore remains poorly understood. In this work, the photooxidation of *n*-dodecane, 1,3,5-trimethylbeneze, and their mixture are studied in the presence of NO_x and SO_2 to mimic the atmospheric oxidation of urban vehicle emissions (including diesel and gasoline vehicles), and the formation of ozone and secondary aerosols are investigated. It is found that ozone formation is enhanced by higher OH concentration and higher temperature, but is influenced little by SO_2 concentration. However, SO_2 can largely enhance the particle formation in both number and mass concentrations, likely due to the promoted new particle formation and acid-catalyzed heterogeneous reactions from the formation of sulfuric acid. In addition, organo-sulfates and organo-nitrates are detected in the formed particles, and the presence of SO_2 can promote the formation of organo-sulfates. These results provide a scientific basis for systematically evaluating the effects of SO_2, OH concentration, and temperature on the oxidation of mixed organic gases in the atmosphere that produce ozone and secondary particles.

1 Introduction

Atmospheric fine particulate matter with diameters < 2.5 μm ($PM_{2.5}$) is a common air pollutant that has a variety of adverse health outcomes (Requia et al., 2018; Tsai et al., 2013; Crouse et al., 2012). Organic aerosol (OA) is an important type of $PM_{2.5}$, and secondary organic aerosol (SOA) accounts for more than 50% of OA by mass concentration (S. Guo et al., 2010; Huang et al., 2014; Jimenez et al., 2009; Kanakidou et al., 2005). In China, concentrations of $PM_{2.5}$ have declined with the implementation of stringent emission control measures since 2013 (Gao et al., 2020; Zhang et al., 2019; Cheng et al., 2019).

https://doi.org/10.5194/acp-2022-294
Preprint. Discussion started: 25 April 2022

The level of primary organic aerosol (POA) in $PM_{2.5}$ has been greatly reduced, however, the contribution of SOA to $PM_{2.5}$ has increased (Ming et al., 2017), highlighting the increasing importance of research on SOA.

Intermediate volatile organic compounds (IVOCs) have been found to contribute to a large fraction of SOA in both field observations (Fang et al., 2021; Wang et al., 2020a; Xu et al., 2020) and laboratory studies (Hu et al., 2021; Cai et al., 2019; Li et al., 2019a; Li et al., 2019b). Long-chain alkanes, as representatives of IVOCs, their laboratory studies mainly include the case of a single precursor or a mixture of multiple precursors. Studies of single long-chain alkanes include reaction kinetics (Lamkaddam et al., 2019; Shi et al., 2019a; Shi et al., 2019b), reaction mechanism (Li et al., 2020; Li et al., 2021a; Li et al., 2017b), analysis of gas phase and particle phase products (Fahnestock et al., 2015; Lamkaddam et al., 2020), quantification of particle yield (Docherty et al., 2021; Loza et al., 2014), and particle physicochemical properties (Li et al., 2017b; Li et al., 2020; Li et al., 2021a), etc. Researches on the mixture of various precursors take long-chain alkanes as one of the species in the actual atmospheric environment, bituminous coal combustion, heavy oil evaporation, and vehicle exhaust, focusing on the chemical composition of the mixture gases, the properties of total organic carbon, the amount of SOA generated, and the effect of S/IVOCs on the formation of SOA contribution (Qi et al., 2021; Hu et al., 2021; Qi et al., 2019; Cai et al., 2019; Deng et al., 2017; Li et al., 2021d; Li et al., 2019a; Li et al., 2019b), etc. However, laboratory studies on the mixture of long-chain alkanes and aromatic hydrocarbons are very limited (Li et al., 2021b), despite both of them being important SOA precursors in vehicle exhaust emissions (Qi et al., 2021).

As an important chemical component of inorganic pollutants in China, SO_2 has a high concentration in the urban atmosphere (Chu et al., 2016; Liu et al., 2016; Liu et al., 2017; Wang et al., 2019). Field observations in North China Plain showed that during heavy haze pollution episodes, SO_2 concentration could be >100 ppb, and the formation and growth rates of SOA and sulfate were much faster than that during clean periods (Li et al., 2017a). Laboratory studies demonstrated that the presence of SO_2 could enhance the SOA formation from anthropogenic and biogenic precursors, e.g., monoterpenes, isoprene, aromatics, etc. (Liggio and Li, 2013; Santiago et al., 2012; Tadeusz E. Kleindienst et al., 2006; Zhang et al., 2020; Yang et al., 2020; Liu et al., 2019). In addition, the presence of SO_2 could affect the light scattering and absorption properties of formed SOA (Zhang et al., 2020; Jaoui et al., 2008; Nakayama et al., 2015; Nakayama et al., 2018). It should be noted that most of the previous studies focused on the effect of SO_2 on the particle formation from single precursor. However, the studies on the impact of SO_2 on particle formation in mixture systems are very limited, although it has important atmospheric implications in better understanding the complex chemical processes in urban areas.

In this work, a large outdoor smog chamber was applied to investigate the effects of SO_2 on particle formation from the mixture of *n*-dodecane and 1,3,5-trimethylbeneze (1,3,5-TMB) in the presence of NO_x. Ozone and particle formation were analyzed in combination with the corresponding equipment. The results in this work are helpful to improve our understanding of the effect of inorganic gases on anthropogenic mixture organic compounds.

https://doi.org/10.5194/acp-2022-294
Preprint. Discussion started: 25 April 2022

2 Experimental Section

2.1 Smog chamber experimental conditions

The experiments were performed in a 56 m^3 outdoor smog chamber, which was built on the rooftop of a building located at Chinese Research Academy Environmental Sciences (CRAES). The details of the chamber have been described elsewhere (Li et al., 2021c). Briefly, fluorinated ethylene propylene Teflon film (FEP 100, DuPont USA) was used as the reactor wall. Sunlight was the natural light source, and a J_{NO2} filter radiometer (Metcon, Germany) was used to detect the irradiation intensity inside the chamber. The variation of temperature (T) and relative humidity (RH) inside the chamber were detected by a temperature and humidity sensor (Beijing Star Sensor Technology Co., LTD.). Three fans were located on the opposite corner of the bottom of the chamber, which were used to mix the gas compounds and seed particles sufficiently. Before each experiment, the chamber was flushed with zero air for at least 24 hours with a flow rate of 200 L min^{-1}. A schematic of the experimental setup is shown in Figure S1.

All the experiments in this work were performed in winter, of which the initial conditions and results were summarized in Table S1 and S2. The entire photochemical reaction process for the conducted experiments lasted 7 hours; the enclosure was opened between 9:00-10:00 in the morning and closed at 16:30-17:30 in the afternoon. Temperature inside the chamber at noon was around 15-30 ℃, and the relative humidity during the whole photochemical process was <15%.

The gas-phase *n*-dodecane and/or 1,3,5-TMB was introduced into the chamber by zero air with a known volume of liquid *n*-dodecane and/or 1,3,5-TMB, and the injector was heated gently during the sample injection process. NO_x was used as the OH precursor: for classics high-NO_x experiments, NO was introduced from a 500 ppm standard gas cylinder; for HONO experiments, HONO was prepared by the dropwise addition of 1 mL 5 wt% $NaNO_2$ into 2 mL 30 wt% H_2SO_4 in a home-made glass bubbler, and the formed NO, NO_2, and HONO was flushed into the chamber with zero air. The measured initial NO_x concentration in the chamber was in the range of 315~445 ppb. SO_2 was introduced from a 60 ppm standard gas cylinder. For experiments with low SO_2 concentration (L-HONO/NO-experiments), initial SO_2 concentration was in the range of 0~9.5 ppb; for experiments with high SO_2 concentration (H-HONO/NO-experiments), initial SO_2 concentration was in the range of 25.5~106 ppb. When the target species introduced into the chamber were mixed evenly, the enclosure of the chamber was open and the reaction started.

2.2 Online and offline measurements

Gaseous NO_x, SO_2, and O_3 concentration inside the chamber were monitored in real time by an SO_2 analyzer (EC 9850, Ecotech, Australia), an O_3 analyzer (EC 9830, Ecotech, Australia), and a NO_x analyzer (EC 9841, Ecotech, Australia), respectively. A HONO analyzer (Chen et al., 2020) (Beijing Zhichen Technology Co., Ltd.) was used to measure the HONO concentration during the reaction process. Organic precursors in the chamber were collected with the Tenax TA solid adsorbent before and after the photochemical reactions, and were then analyzed with a thermal desorption–gas chromatography with flame ionization detection (GC, 8890; TD, UNITY-xr).

The formed particles were monitored with a scanning mobility particle sizer (SMPS, Model 3080, Model 3081, and Model 3772, TSI Inc., USA). The particles were also collected with a low-flow sampler (LV 40BW, Sibata Scientific Technology Ltd., Soka, Japan) at a flow rate of 15 L min^{-1} for 20 min with PTFE filters (0.2 μm, 47 mm, Merck Millipore, type FGLP). The collected PTFE filters were extracted with methanol and analyzed with electrospray ionization quadrupole time-of flight mass spectrometry (ESI-Q-ToF-MS, Bruker Compact). The concentration of inorganic species in aerosols and gases for mixture experiments in the chamber were measured with a Monitor for AeRosols and Gases in Ambient air (MARGA 2080, Applikon, Metrohm). The attenuated total internal reflection infrared (ATR-IR) analysis was used to measure the potential functional groups in filter extracts; an FTIR spectrometer (Bruker, Tensor 27) equipped with a RT-DLaTGs detector was applied.

2.3 Calculation methods of SOA yields and OH concentration

Details of the calculation methods of wall-loss corrections and secondary aerosol (SA) yields can be referred to Li et al. (2021b). Briefly, when calculating the SA yields, the organic vapor and aerosol wall-loss corrections were both considered (Zhang et al., 2014). The ratio of average gas-particle partitioning timescale ($\bar{\tau}_{g-p}$) to the vapor wall-loss timescale ($\bar{\tau}_{g-w}$) could be used to evaluate the organic vapor wall-loss correction (Chen et al., 2019). The particle wall-loss was corrected based on the size-dependent coefficients from inert particle (ammonium sulfate) wall-loss experiments, which can be referred to Li et al. (2021c).

In this work, the hydroxyl free radical (OH) was determined by measuring the concentration of 1,3,5-trimethylbeneze by TD-GC during the mixture experiments (Barmet et al., 2012). Changes in the 1,3,5-trimethylbeneze concentration over time can be expressed as:

$$\frac{d[1{,}3{,}5-trimethylbeneze]}{dt} = -k[OH][1{,}3{,}5-trimethylbeneze] \quad (1)$$

where k is the rate constant for the reaction of 1,3,5-trimethylbeneze and OH radical. The rate constants (Atkinson and Arey, 2003) at 298 K for reaction of 1,3,5-trimethylbenzene with OH radical is 5.67 × 10^{-11} cm^3 molecule^{-1} s^{-1}. In the case of constant OH radical concentration level, equation (1) can be integrated to equation (2):

$$\ln[1{,}3{,}5-trimethylneneze]_0 = k[OH]t + \ln[1{,}3{,}5-tirmethylbeneze]_t \quad (2)$$

Plotting the natural logarithm (ln) of the 1,3,5-trimethylbeneze versus time (t)，the slope that equals to k[OH] is obtained. Therefore, average OH radical concentration during each period is expressed as:

$$[OH] = \frac{slope}{k} \quad (3)$$

https://doi.org/10.5194/acp-2022-294
Preprint. Discussion started: 25 April 2022

Atmospheric Chemistry and Physics Discussions

3 Results and Discussions

3.1 General results of the experiments

The HONO experiments were conducted as follows: 1,3,5-TMB + HONO + SO_2 (HONO-TMB), *n*-dodecane + HONO + SO_2 (HONO-Dod), 1,3,5-TMB + *n*-dodecane + HONO + SO_2 (HONO-Mix). The concentration of organic precursor was 137.9~216.9 ppb for 1,3,5-TMB and 23.2~28.9 ppb for *n*-dodecane. The measured NO_x concentration applied in HONO experiments was in the range of 315~429 ppb. According to Ng et al. (2007), this method could generate (6.3~8.6) × 10^6 molecules cm^{-3} OH initially. As shown in Figure 1a, the concentration of OH radicals generated at the beginning of the experiment is in the range of (1.03~1.23) × 10^7 molecules cm^{-3}, which is slightly higher than that of Ng et al. (2007). The OH exposure was in the range of 3.74 × 10^{10} to 7.16 × 10^{10} molecules cm^{-3} s, as revealed in Figure 1b, corresponding to 6.9~13.3 simulated hours, assuming a global average OH concentration of 1.5 × 10^6 molecules cm^{-3} (Mao et al., 2009). The reaction profiles of the HONO experiments are shown in Figure S2.

The NO experiments were conducted as follows: 1,3,5-TMB + NO + SO_2 (NO-TMB), *n*-dodecane + NO + SO_2 (NO-Dod), 1,3,5-TMB + *n*-dodecane + NO + SO_2 (NO-Mix). The concentration of organic precursor was 177.8~192.4 ppb for 1,3,5-TMB and 23~29.9 ppb for *n*-dodecane. The initial NO_x concentration in the chamber was in the range of 212~355 ppb, resulting in the estimated OH concentration of (3.4~4.9) × 10^6 molecules cm^{-3}, as shown in Figure 1. Using the OH concentration above, the calculated photochemical age from these experiments was in the range of 0.9~11.9 hours. The reaction profiles of the NO experiments are shown in Figure S3.

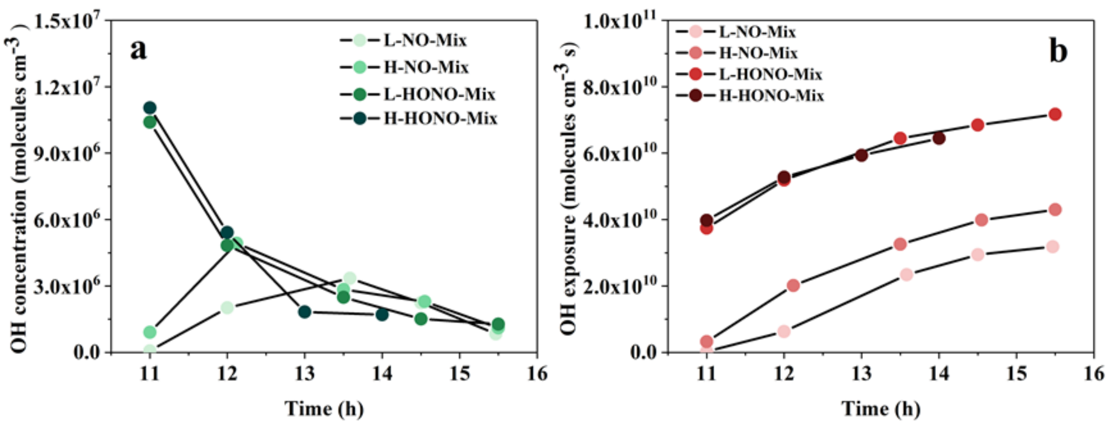

Figure 1. (a) OH radical concentration and (b) OH exposure versus time (hour) for mixture experiments.

3.2 Ozone formation and gas phases products

3.2.1 Ozone formation

The ozone formation in the NO and HONO experiments are shown in Figure S2 and S3. In order to conduct a specific analysis, the highest concentration of ozone generated by each reaction is selected and shown in Figure 2. It can be clearly

https://doi.org/10.5194/acp-2022-294
Preprint. Discussion started: 25 April 2022

seen that the addition of SO_2 has little effect on ozone generation, and the ozone generation was analyzed below from the perspective of the type of precursors, VOCs/NO_x, temperature, and the type of oxidant.

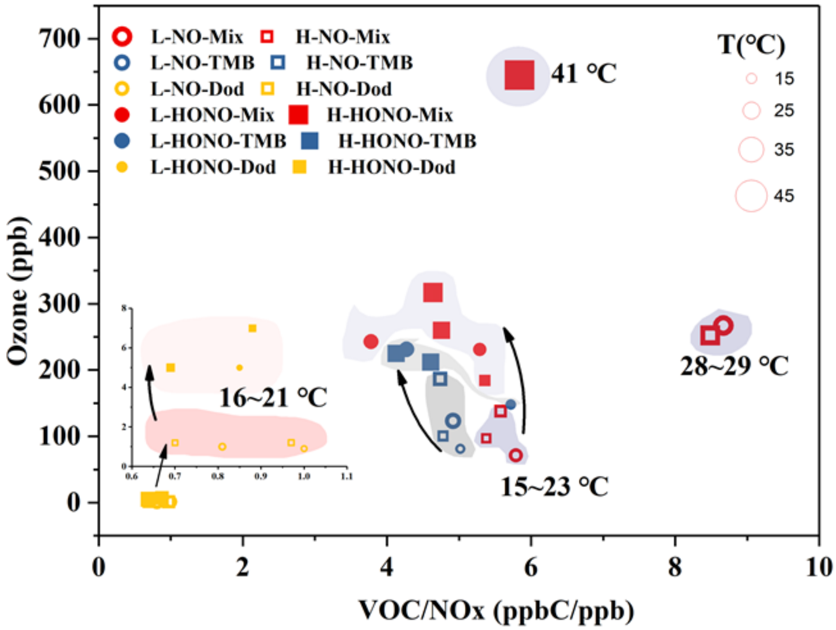

Figure 2. Ozone formation in the NO and HONO experiments. The temperature (T) and ozone concentration here refers to the maximum value during the reaction process. The pink area refers to NO-Dod experiments, and the light pink area refers to HONO-Dod experiments; the grey area refers to NO-TMB experiments, and the light grey area refers to HONO-TMB experiments; the purple area refers to NO-Mix experiments, and the light purple area refers to HONO-Mix experiments.

According to previous studies, the photochemical ozone formation potentials (OFP) of VOCs are sensitive to their rate constants with OH radicals, i.e., VOCs with high reactivities have greater contributions to the ozone formation in the ambient atmosphere (Jenkin and Hayman, 1999). The reaction rate constants with OH at 298 K for 1,3,5-TMB and *n*-dodecane are 5.67×10^{-11} cm^3 $molecule^{-1}$ s^{-1} and 1.39×10^{-11} cm^3 $molecule^{-1}$ s^{-1}, respectively (Sivaramakrishnan and Michael, 2009; Atkinson and Arey, 2003). As shown in Figure 2, compared with the mixture and 1,3,5-TMB reaction systems, the ozone concentration generated by the *n*-dodecane system is very low (< 8 ppb). For *n*-dodecane experiments, the formed ozone concentration under HONO condition, the light pink area, is higher than that under NO condition, the pink area; for 1,3,5-TMB experiments, the ozone concentration under HONO condition in the light grey area is higher than that under NO conditions; the mixture experiments also show the similar phenomenon, the ozone concentration in light purple area is higher than that in purple area. This can also be explained by the OH exposure: as shown in Figure 1, for similar NO_x concentration, HONO conditions have higher OH radicals than NO experiments. Higher OH radicals would make the reaction system more oxidative, forming more RO_2 and HO_2 that can react with NO. This leads to the competition to the reaction O_3+NO → NO_2 +O_2, and causes the accumulation of ozone. It is also shown in Figure 2 that the VOC to NO_x ratio (within the range of 1~10

https://doi.org/10.5194/acp-2022-294
Preprint. Discussion started: 25 April 2022

ppbC/ppb) has little effect on the generation of ozone. However, temperature has a great influence on the formation of ozone. For experiment H-HONO-Mix-3, the temperature at noon was 41 °C, with a maximum ozone concentration of 645 ppb. In contrast, for the mixture experiments under similar VOC/NOx conditions but lower temperature (16~27°C), the ozone concentration was 184~317 ppb. The reaction rates with OH increase with the rise of temperature (Atkinson and Arey, 2003), which in turn accelerate the oxidation processes. This may be a possible reason for the higher concentration of ozone generated under higher temperature conditions.

3.2.2 HONO concentration

For HONO experiments, HONO was introduced into the chamber with the same operation procedure, leading to similar HONO concentration. As shown in Figure 3a, initial HONO concentrations exceed the device detection limit (70 ppb). When the enclosure was open, the HONO concentration decreased rapidly with the progress of the reaction in the first two hours.

For NO experiments, the concentration of HONO first slowly increased at about 1 h after the photochemical reaction started, and then decreased (Figure 3b). At the same time, the particles began to increase significantly after 1 hour to 2 hours after the start of the reaction, as revealed in Figure S4. The increase in HONO may have two reasons: the gas-phase reaction of NO with OH radicals and the heterogeneous reactions of NO_2 (Alicke, 2002; Wall and Harris, 2016). The concentration of HONO generated in the mixture and 1,3,5-trimethylbeneze experiments is slightly lower than that in the *n*-dodecane experiment, and the mixture experiments have the lowest HONO concentration. This is likely due to the difference in OH reactivity: the OH reactivity in the n-dodecane experiments (7.8-10.2 s^{-1}) is much lower than that in the 1,3,5-TMB (255-267.4 s^{-1}) and mixture experiments (255.9-278.6 s^{-1}), leading to weaker competition to OH+NO reaction.

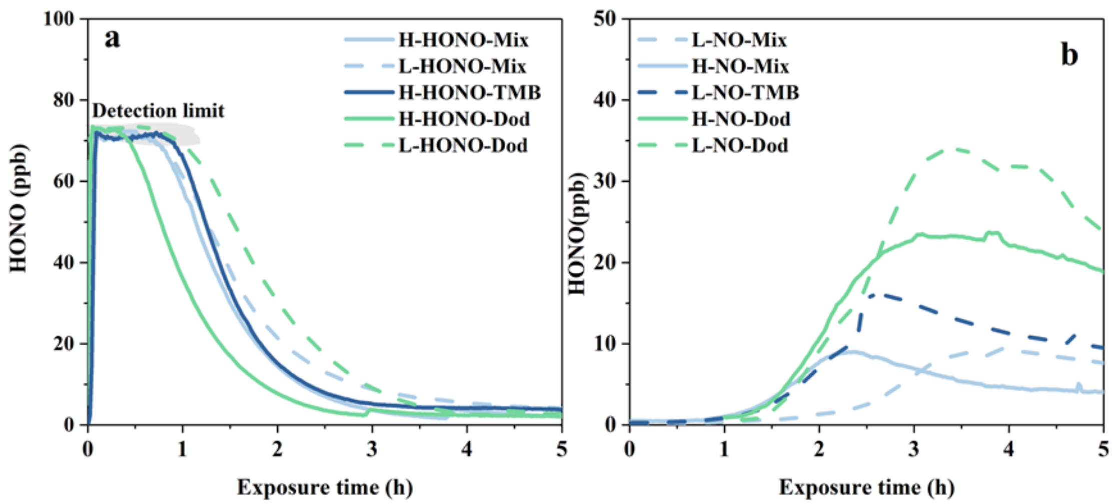

185 **Figure 3. HONO concentration versus time during conducted experiments.**

3.3 Effect of NO_x and SO_2 on particle formation

The particle formation (size distribution and max number concentration) in the NO and HONO experiments are shown in Figures S4 and S5, and the corresponding max mass concentrations are shown in Figure 4. It is shown that the higher SO_2 concentration can promote particle production in both number (Figures S4 and S5) and mass (Figure 4) concentration. This finding is similar to previous studies with single precursors (Liu et al., 2016; Liu et al., 2019), and is likely due to the formation of sulfuric acid from SO_2 oxidation. First, sulfuric acid can participate in nucleation and enhance the new particle formation (Sipila et al., 2010), resulting in higher particle number concentration. Second, sulfuric acid can promote the acid-catalyzed heterogeneous reactions and enhance the uptake of reactive organic compounds (Liu et al., 2016; Jang et al., 2002; Cao and Jang, 2007), which may lead to higher particle mass concentration. At last, the presence of SO_2 and sulfuric acid favour the formation of organo-sulfates (Liu et al., 2019; Liu et al., 2017; Chu et al., 2016), which is detected in our experiments (see Section 3.4).

In addition, it is found that the maximum values of particle number and mass concentration in the HONO reaction systems are higher than that of the NO reaction systems. In other words, under similar NO_x concentrations, HONO conditions would be beneficial to the formation of particles, with either low SO_2 or high SO_2 concentration. This phenomenon can be explained by the higher OH concentration in HONO experiments, as shown in Figure 1. Higher OH concentration causes the higher consumption rate of the precursors and the subsequent faster particle generation rates.

Figure 4 also shows the temperature effect on particle formation. For the same precursor, under the similar VOC/NOx conditions, it can be seen that the lower the temperature, the higher the mass of particulate matter. Lower temperatures can affect the partitioning process of organic vapors and facilitate the formation of particles, which in turn increases the particle mass concentration in the reaction system, and this is consistent with previous experimental reports (Ding et al., 2017; Li et al., 2020; Sheehan and Bowman, 2001; Takekawa et al., 2003; Warren et al., 2009). Meanwhile, it can be seen that with the increase of the VOC/NO_x ratio value, the particle mass concentration increases (Wang et al., 2020b; Li et al., 2017c).

https://doi.org/10.5194/acp-2022-294
Preprint. Discussion started: 25 April 2022

Atmospheric Chemistry and Physics Discussions
Open Access
EGU

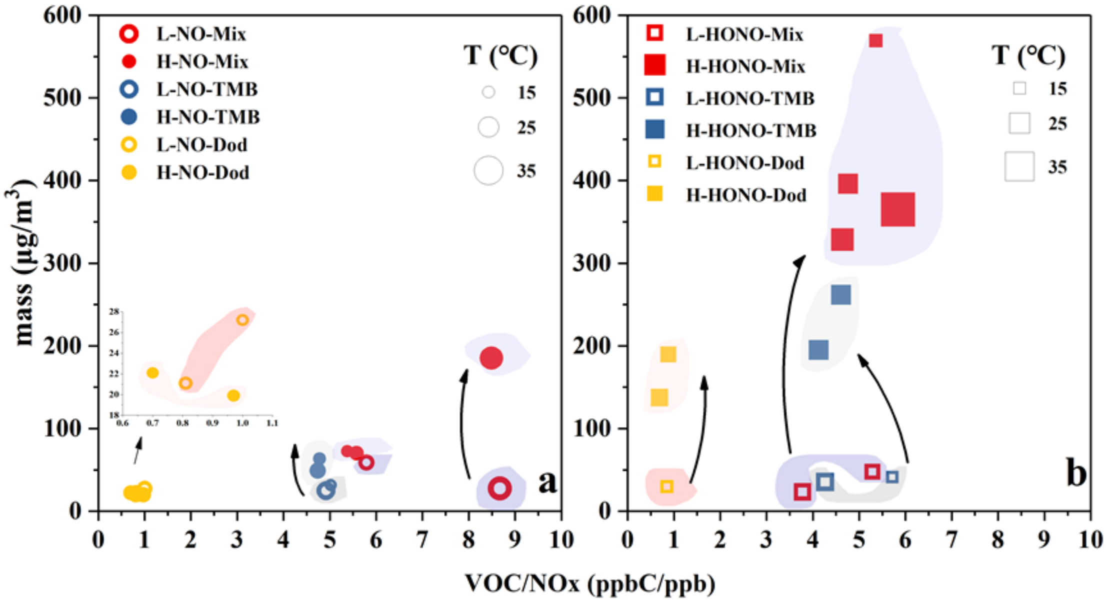

Figure 4. Particle formation of NO and HONO experiments. The temperature (T) and particle mass concentration here refers to the maximum value during the reaction process. The pink area refers to L-NO-Dod or L-HONO-Dod experiments, and the light pink area refers to H-NO-Dod or H-HONO-Dod experiments; the grey area refers to L-NO-TMB or L-HONO-TMB experiments, and the light grey area refers to H-NO-TMB or H-HONO-TMB experiments; the purple area refers to L-NO-Mix or L-HONO-Mix experiments, and the light purple area refers to H-NO-Mix or H-HONO-Mix experiments.

3.4 Chemical Compositions of Particles

3.4.1 Inorganic chemical components

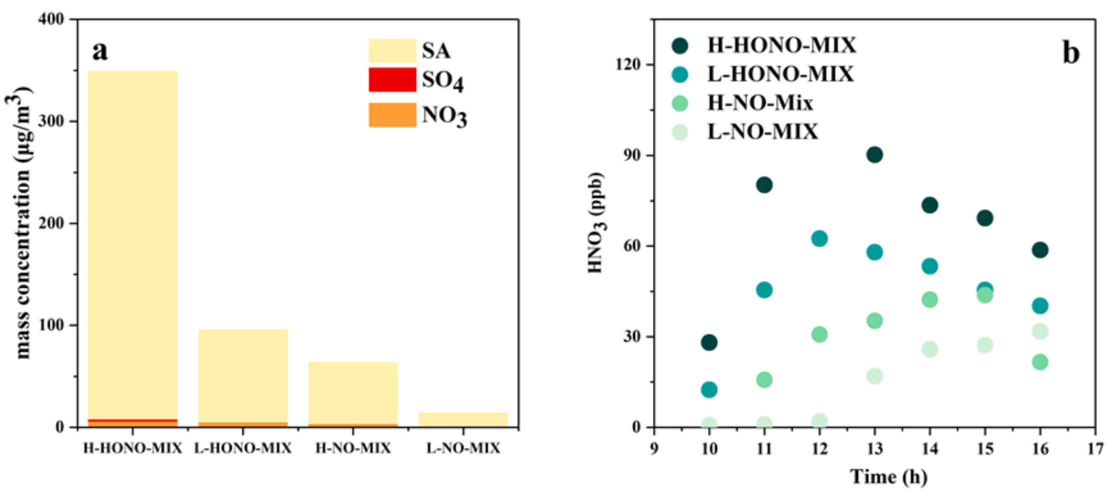

https://doi.org/10.5194/acp-2022-294
Preprint. Discussion started: 25 April 2022

Figure 5. (a) The measured mass concentration of sulfate, nitrate, and total secondary aerosol in the particle phase. The data used in this plot are the average of the hour in which the mass concentration was the greatest. (b) The concentration of gas-phase nitric acid in the mixture system.

We analyzed the inorganic components and organic components of the generated particles respectively. Compared with the single-precursor systems, the particle mass concentration generated by the mixture system is the highest, so we selected the mixture system as the target and analyzed the inorganic components. Overall, the amounts of sulfate and nitrate of HONO-Mix experiments are higher than that of NO-Mix experiments (HONO-Mix > NO-Mix). In the above reaction system, the generation pathway of nitric acid is mainly the reaction (Jarvis et al., 2009): $NO_2 + OH \rightarrow HNO_3$. With the similar NO_x concentration, higher OH radicals are beneficial to the generation of nitric acid. As shown in Figure 1, the HONO-Mix system has higher concentration of OH radicals, which can explain the higher concentration of gas-phase nitric acid (Figure 5b) and nitrate aerosol in this system ($\text{HONO-Mix}_{nitrate}$ > $\text{NO-Mix}_{nitrate}$). When SO_2 is added to the chamber, sulfate is formed by photooxidation of SO_2 in the reaction initiated by OH radical (Wang et al., 2021; Liu et al., 2017) ($\text{HONO-Mix}_{sulfate}$ > $\text{NO-Mix}_{sulfate}$). For HONO experiments, the amounts of sulfate and nitrate of H-HONO-Mix are higher than that of L-HONO-Mix (H-HONO-Mix > L-HONO-Mix), especially for sulfate. As mentioned above, higher OH concentration is beneficial to nitrate formation, and higher SO_2 will promote the formation of sulfate in the system. While for NO experiments, the amounts of sulfate and nitrate of H-NO-Mix are also higher than that of L-NO-Mix (H-NO-Mix > L-NO-Mix), with L-NO-Mix experiment forming negligible sulfate and nitrate. As shown in Figure 1, L-NO-Mix has the lowest OH exposure, and the SO_2 concentration is also low, this can explain its low nitrate and sulfate concentration.

As shown in Figure 5a, compared with the total mass concentration of the resulting particles, the sulfate and nitrate production amounts under the four conditions are very low, so we focus on analyzing the organic components in the particles, including the analysis of functional groups by infrared spectroscopy and the analysis of chemical components by mass spectrometry.

3.4.2 Inorganic chemical components

In order to analyze the functional groups of the particles, we dissolved the collected particles with methanol and detected them with an infrared spectrometer. Figure S6 shows the IR spectra of aerosols formed under NO conditions and HONO conditions. According to the positions of the absorption peak in the IR spectra, different functional groups were assigned. The bold peak at 3360 cm^{-1} is assigned to the characteristic peak of C-OH in alcohol, the broadband at 3100-3300 cm^{-1} (3192 cm^{-1}) originates from the O-H stretching vibration of hydroxyl and carboxyl groups (Liu et al., 2017; Coury and Dillner, 2008), and the peaks around 1633-1660 cm^{-1} are assigned to the C=O stretching vibrations of ketones, aldehydes, and carboxylic acids (Coury and Dillner, 2008). The peaks at 2960 cm^{-1} corresponds to CH_3 stretching vibration in alkanes, 2921 cm^{-1} and 2850 cm^{-1} corresponds to CH_2 stretching vibration in alkanes, and the broadbands around 1415-1465 cm^{-1} represent the deformation vibrations of methylene and methyl groups. The peak at 1268 cm^{-1} is assigned to the -ONO_2 stretching in

https://doi.org/10.5194/acp-2022-294
Preprint. Discussion started: 25 April 2022

nitrate ester (Jia and Xu, 2014; Li et al., 2021b). According to literature reports, peaks in the range of 1000-1200 cm^{-1} is assigned to the absorption peak of sulfate (Wu et al., 2013), peaks around 1040-1070 cm^{-1} represent the absorption band of S=O in organic compound (Chihara, 1958), peak at 1100 cm^{-1} corresponds to the sulfate in sulfate and organic compounds (Liu et al., 2017). The above analysis confirmed the presence of carboxylic acids, alcohols, nitrates, sulfates, aldehydes and ketones in aerosols derived from both the NO and HONO conditions with high or low SO_2.

In order to conduct a more in-depth analysis of the organic compounds in the particles, we performed the mass spectrometry analysis (Figure 6). In a previous study (Li et al., 2021b), we have shown that the chemical interactions between intermediate products from n-dodecane and 1,3,5-TMB can promote particle formation in the mixure experiments under the HONO conditions. In this study, we focus on the influence of SO_2 and the concentration of OH radicals on the formation of particles, and analyzed the formed particles of mixture experiments.

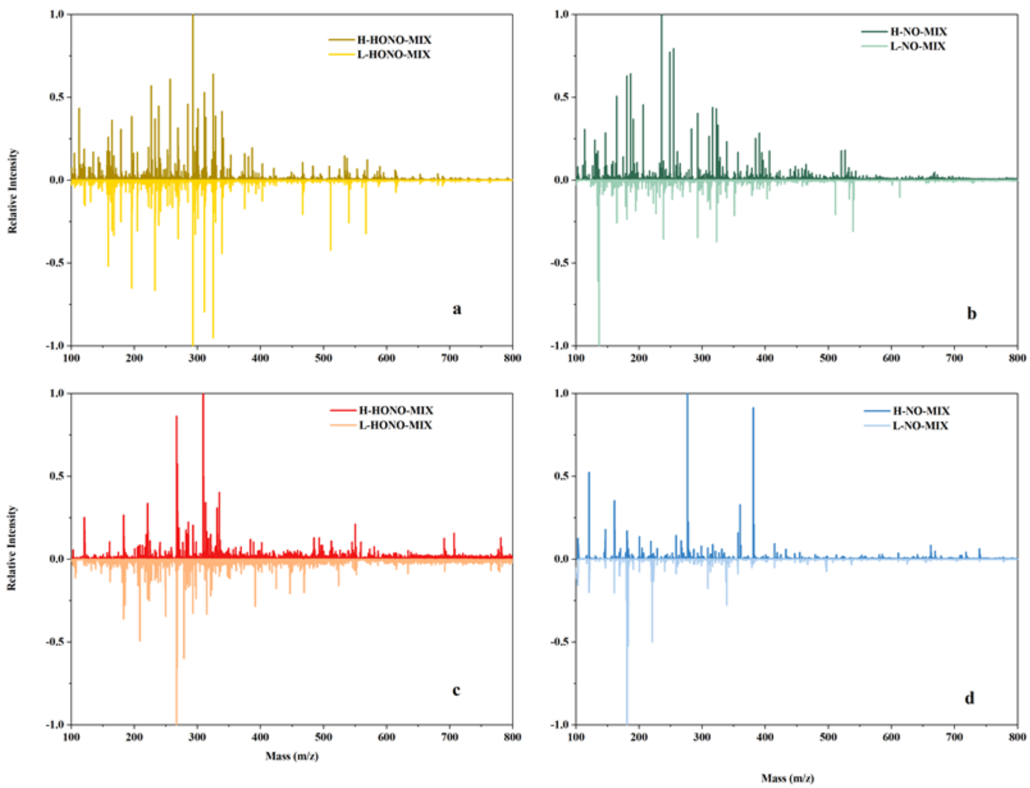

Figure 6. Mass spectra of mixture experiments (a) HONO mixture experiments in negative mode; (b) NO mixture experiments in negative mode; (c) HONO mixture experiments in positive mode; (d) NO mixture experiments in positive mode. The y axis is the relative intensity normalized by dividing by the maximum signal strength of the mass spectra.

The products of mixture experiments were detected by ESI-Q-ToF-MS in both negative (Figure 6 a,b) and positive (Figure 6 c,d) mode. Compared to NO-Mix, more products with larger molecular weights are formed under HONO-Mix. This is probably due to the higher OH concentration in the HONO experiments (Figure 1), which favours the formation of

https://doi.org/10.5194/acp-2022-294
Preprint. Discussion started: 25 April 2022

large molecular weight products through functionalization reactions. Lambe et al. (2012) reported that when the OH radical exposure was within (5~6) × 10^{11} mole cm^{-3} s, the SOA yield of alkanes precursors (C_{10} and C_{15}) exhibited an increase as a function of OH radical exposure, and the increase correlated with an increase in oxygen content.

Meanwhile, organo-sulfates and organo-nitrates are formed in the mixture experiments, as shown in Table S3. It is found that more organo-nitrates are formed under HONO conditions compared with NO conditions. The primary formation pathway of organo-nitrates is the reaction of RO_2 + NO, and the RO_2 is mainly formed through the reaction of organic gases with OH radical (Li et al., 2022; Tsiligiannis et al., 2019). Under HONO conditions, higher concentration of OH radical is formed (Figure 1), so more RO_2 will exist in HONO experiments, and thus more organo-nitrates will be formed. In addition, high SO_2 conditions are more conducive to the formation of organo-sulfates, e.g., H-NO-$Mix_{organo\text{-}sulfate}$ > L-NO-$Mix_{organo\text{-}sulfate}$ (Table S3). As discussed in section 3.4.1, sulfate is formed by reaction of SO_2 + OH radical (Wang et al., 2021; Liu et al., 2017), and higher SO_2 would facilitate the formation of sulfate in the experiments. According to previous studies (Yang et al., 2020), organo-sufates are mainly formed through the reaction of sulfate with compound containing OH bonds or ether bonds. Therefore, higher SO_2 would facilitate the formation of organo-surfates.

4 Conclusion and implications

In the present work, a large-scale outdoor smog chamber was applied to study the effect of inorganic gases (SO_2 and NO_x) on the photochemical process of mixed anthropogenic organic gases, i.e., *n*-dodecane and 1,3,5-trimethylbeneze. The OH concentration under the HONO conditions is higher than that under the classic NO_x conditions at similar measured NO_x concentration. The ozone formation is affected by the reaction precursors, the concentration of OH radicals, and the temperature: precursors with higher ozone formation potential also contribute significantly to ozone formation in the mixture reaction system; higher temperature and higher OH concentration are beneficial to the formation of ozone in the reactions. In contrast, the presence of SO_2 has little effect on the concentration of ozone.

However, the presence of SO_2 can greatly promote the formation of particles in both number and mass concentration, likely due to the enhanced new particle formation and acid-catalyzed heterogeneous reactions from the formation of sulfuric acid and the formation of organo-sulfates (Liu et al., 2019; Liu et al., 2017; Li et al., 2017c). In addition, higher OH radical concentration and lower temperature are also beneficial to the formation of particles. For the particle composition, the content of inorganic nitrate and sulfate under the HONO conditions was higher than that under the NO conditions, although organic aerosols dominate the total secondary aerosols. The organo-sulfates and organo-nitrates are detected in the formed particles, and the presence of SO_2 is found to promote the formation of organo-sulfates.

This study provides the first attempt to investigate the role of SO_2 in the oxidation of mixed anthropogenic organic gases with various OH concentrations and temperature conditions. The results here can improve our understanding in the chemical processes that lead to ozone and secondary particle formation in the complex urban areas influenced by complex emissions (including vehicle exhaust, coal combustion, etc.). More in-depth and detailed research on the mixture reaction systems with atmospheric-relevant conditions should be carried out in the future to deepen our understanding of the physical and chemical processes in the oxidation of organic vapors in the real atmosphere.

Data availability. The data used in this study are available upon request from the corresponding author.

Author contributions. JLL, HL, and MFG designed the experiments; JLL conducted the experiments with help from HZ, XZ, YYJ, WHC and YXK; JLL analyzed the data and wrote the paper, with contributions from KL, HL and MFG; and YXC, YQR, YJZ, HJZ, RG, ZHW, FB, XC, XZW, and WGW commented on the paper.

Competing interests. The authors declare that they have no conflict of interest

Financial support. This research has been supported by the National Natural Science Foundation of China (Contract No. 42130606), Special fund project of Guangdong Provincial Department of Ecology and Environment, the Beijing Municipal Science & Technology Commission (Grant no. Z181100005418015), National research program for Key issues in air pollution control (DQGG2021301), and the Fundamental Research Funds for Central Public Welfare Scientific Research Institutes of China, Chinese Research Academy of Environmental Sciences (No. 2019YSKY-018).

References

Alicke, B.: Impact of nitrous acid photolysis on the total hydroxyl radical budget during the Limitation of Oxidant Production/Pianura Padana Produzione di Ozono study in Milan, J. Geophys. Res., 107, 10.1029/2000jd000075, 2002.

Atkinson, R. and Arey, J.: Atmospheric degradation of volatile organic compounds, Chem. Rev., 103, 4605-4638, 10.1021/cr0206420, 2003.

Barmet, P., Dommen, J., DeCarlo, P. F., Tritscher, T., Praplan, A. P., Platt, S. M., Prévôt, A. S. H., Donahue, N. M., and Baltensperger, U.: OH clock determination by proton transfer reaction mass spectrometry at an environmental chamber, Atmos. Meas. Tech., 5, 647-656, 10.5194/amt-5-647-2012, 2012.

Cai, S., Zhu, L., Wang, S., Wisthaler, A., Li, Q., Jiang, J., and Hao, J.: Time-resolved intermediate-volatility and semivolatile organic compound emissions from household coal combustion in Northern China, Environ. Sci. Technol., 53, 9269-9278, 10.1021/acs.est.9b00734, 2019.

Cao, G. and Jang, M.: Effects of particle acidity and UV light on secondary organic aerosol formation from oxidation of aromatics in the absence of NOx, Atmos. Environ., 41, 7603-7613, 10.1016/j.atmosenv.2007.05.034, 2007.

Chen, T., Liu, Y., Ma, Q., Chu, B., Zhang, P., Liu, C., Liu, J., and He, H.: Significant source of secondary aerosol: formation from gasoline evaporative emissions in the presence of SO_2 and NH_3, Atmos. Chem. Phys., 19, 8063-8081, 10.5194/acp-19-8063-2019, 2019.

Chen, Y., Wang, W., Lian, C., Peng, C., Zhang, W., Li, J., Liu, M., Shi, B., Wang, X., and Ge, M.: Evaluation and impact factors of indoor and outdoor gas-phase nitrous acid under different environmental conditions, J. Environ. Sci. 95, 165-171, 10.1016/j.jes.2020.03.048, 2020.

Cheng, J., Su, J., Cui, T., Li, X., Dong, X., Sun, F., Yang, Y., Tong, D., Zheng, Y., Li, Y., Li, J., Zhang, Q., and He, K.: Dominant role of emission reduction in $PM_{2.5}$ air quality improvement in Beijing during 2013–2017: a model-based decomposition analysis, Atmos. Chem. Phys., 19, 6125-6146, 10.5194/acp-19-6125-2019, 2019.

Chihara, G.: Characteristic infrared absorption band of organic sulfate esters, Chem. Pharm. Bull., 6, 114, 1958.

Chu, B., Zhang, X., Liu, Y., He, H., Sun, Y., Jiang, J., Li, J., and Hao, J.: Synergetic formation of secondary inorganic and organic aerosol: effect of SO_2 and NH_3 on particle formation and growth, Atmos. Chem. Phys., 16, 14219-14230, 10.5194/acp-16-14219-2016, 2016.

Coury, C. and Dillner, A. M.: A method to quantify organic functional groups and inorganic compounds in ambient aerosols using attenuated total reflectance FTIR spectroscopy and multivariate chemometric techniques, Atmos. Environ., 42, 5923-5932, 10.1016/j.atmosenv.2008.03.026, 2008.

Crouse, D. L., Peters, P. A., van Donkelaar, A., Goldberg, M. S., Villeneuve, P. J., Brion, O., Khan, S., Atari, D. O., Jerrett, M., Pope, C. A., Brauer, M., Brook, J. R., Martin, R. V., Stieb, D., and Burnett, R. T.: Risk of nonaccidental and cardiovascular mortality in relation to long-term exposure to low concentrations of fine particulate matter: a Canadian national-level cohort study, Environ. Health Persp., 120, 708-714, 10.1289/ehp.1104049, 2012.

Deng, W., Hu, Q., Liu, T., Wang, X., Zhang, Y., Song, W., Sun, Y., Bi, X., Yu, J., Yang, W., Huang, X., Zhang, Z., Huang, Z., He, Q., Mellouki, A., and George, C.: Primary particulate emissions and secondary organic aerosol (SOA) formation from idling diesel vehicle exhaust in China, Sci. Total Environ., 593-594, 462-469, 10.1016/j.scitotenv.2017.03.088, 2017.

Ding, X., Zhang, Y. Q., He, Q. F., Yu, Q. Q., Wang, J. Q., Shen, R. Q., Song, W., Wang, Y. S., and Wang, X. M.: Significant Increase of Aromatics-Derived Secondary Organic Aerosol during Fall to Winter in China, Environ. Sci. Technol., 51, 7432-7441, 10.1021/acs.est.6b06408, 2017.

Docherty, K. S., Yaga, R., Preston, W., Jaoui, M., Reidel, T. P., Offenberg, J. H., Kleindienst, T. E., and Lewandowski, M.: Relative contributions of selected multigeneration products to chamber SOA formed from photooxidation of a range (C_{10}-C_{17}) of n-alkanes under high NOx conditions, Atmos. Environ. (1994), 244, 10.1016/j.atmosenv.2020.117976, 2021.

Fahnestock, K. A. S., Yee, L. D., Loza, C. L., Coggon, M. M., Schwantes, R., Zhang, X., Dalleska, N. F., and Seinfeld, J. H.: Secondary organic aerosol composition from C-12 alkanes, J. Phys. Chem. A, 119, 4281-4297, 10.1021/jp501779w, 2015.

Fang, H., Huang, X., Zhang, Y., Pei, C., Huang, Z., Wang, Y., Chen, Y., Yan, J., Zeng, J., Xiao, S., Luo, S., Li, S., Wang, J., Zhu, M., Fu, X., Wu, Z., Zhang, R., Song, W., Zhang, G., Hu, W., Tang, M., Ding, X., Bi, X., and Wang, X.: Measurement report: Emissions of intermediate-volatility organic compounds from vehicles under real-world driving conditions in an urban tunnel, Atmos. Chem. Phys., 21, 10005-10013, 10.5194/acp-21-10005-2021, 2021.

Gao, M., Liu, Z., Zheng, B., Ji, D., Sherman, P., Song, S., Xin, J., Liu, C., Wang, Y., Zhang, Q., Xing, J., Jiang, J., Wang, Z., Carmichael, G. R., and McElroy, M. B.: China's emission control strategies have suppressed unfavorable influences of climate on wintertime PM2.5 concentrations in Beijing since 2002, Atmos. Chem. Phys., 20, 1497-1505, 10.5194/acp-20-1497-2020, 2020.

Hu, W., Zhou, H., Chen, W., Ye, Y., Pan, T., Wang, Y., Song, W., Zhang, H., Deng, W., Zhu, M., Wang, C., Wu, C., Ye, C., Wang, Z., Yuan, B., Huang, S., Shao, M., Peng, Z., Day, D. A., Campuzano-Jost, P., Lambe, A. T., Worsnop, D. R., Jimenez, J. L., and Wang, X.: Oxidation flow reactor results in a Chinese megacity emphasize the important contribution of S/IVOCs to ambient SOA formation, Environ. Sci. Technol., 10.1021/acs.est.1c03155, 2021.

Huang, R. J., Zhang, Y., Bozzetti, C., Ho, K. F., Cao, J. J., Han, Y., Daellenbach, K. R., Slowik, J. G., Platt, S. M., Canonaco, F., Zotter, P., Wolf, R., Pieber, S. M., Bruns, E. A., Crippa, M., Ciarelli, G., Piazzalunga, A., Schwikowski, M., Abbaszade, G., Schnelle-Kreis, J., Zimmermann, R., An, Z., Szidat, S., Baltensperger, U., El Haddad, I., and Prevot, A. S.: High secondary aerosol contribution to particulate pollution during haze events in China, Nature, 514, 218-222, 10.1038/nature13774, 2014.

Jang, M. S., Czoschke, N. M., Lee, S., and Kamens, R. M.: Heterogeneous atmospheric aerosol production by acid-catalyzed particle-phase reactions, Science, 298, 814-817, 10.1126/science.1075798, 2002.

Jaoui, M., Edney, E. O., Kleindienst, T. E., Lewandowski, M., Offenberg, J. H., Surratt, J. D., and Seinfeld, J. H.: Formation of secondary organic aerosol from irradiated alpha-pinene/toluene/NOx mixtures and the effect of isoprene and sulfur dioxide, J. Geophys. Res.-Atmos., 113, 10.1029/2007jd009426, 2008.

Jarvis, J. C., Hastings, M. G., Steig, E. J., and Kunasek, S. A.: Isotopic ratios in gas-phase HNO_3 and snow nitrate at Summit, Greenland, J. Geophys. Res., 114, 10.1029/2009jd012134, 2009.

Jenkin, M. E. and Hayman, G., D.: Photochemical ozone creation potentials for oxygenated volatile organic compounds: sensitivity to variations in kinetic and mechanistic parameter, Atmos. Environ., 33, 1275-1293, 1999.

Jia, L. and Xu, Y.: Effects of Relative Humidity on ozone and secondary organic aerosol formation from the photooxidation of benzene and ethylbenzene, Aerosol Sci. Tech., 48, 1-12, 10.1080/02786826.2013.847269, 2014.

Jimenez, J. L., Canagaratna, M. R., Donahue, N. M., Prevot, A. S., Zhang, Q., Kroll, J. H., DeCarlo, P. F., Allan, J. D., Coe, H., Ng, N. L., Aiken, A. C., Docherty, K. S., Ulbrich, I. M., Grieshop, A. P., Robinson, A. L., Duplissy, J., Smith, J. D., Wilson, K. R., Lanz, V. A., Hueglin, C., Sun, Y. L., Tian, J., Laaksonen, A., Raatikainen, T., Rautiainen, J., Vaattovaara, P., Ehn, M., Kulmala, M., Tomlinson, J. M., Collins, D. R., Cubison, M. J., Dunlea, E. J., Huffman, J. A., Onasch, T. B., Alfarra, M. R., Williams, P. I., Bower, K., Kondo, Y., Schneider, J., Drewnick, F., Borrmann, S., Weimer, S., Demerjian, K., Salcedo, D., Cottrell, L., Griffin, R., Takami, A., Miyoshi, T., Hatakeyama, S., Shimono, A., Sun, J. Y., Zhang, Y. M., Dzepina, K., Kimmel, J. R., Sueper, D., Jayne, J. T., Herndon, S. C., Trimborn, A. M., Williams, L. R., Wood, E. C., Middlebrook, A. M., Kolb, C. E., Baltensperger, U., and Worsnop, D. R.: Evolution of organic aerosols in the atmosphere, Science, 326, 1525-1529, 10.1126/science.1180353, 2009.

Kanakidou, M., Seinfeld, J. H., Pandis, S. N., Barnes, I., Dentener, F. J., Facchini, M. C., Dingenen, R. V., Ervens, B., Nenes, A., Nielsen, C. J., Swietlicki, E., Putaud, J. P., Balkanski, Y., Fuzzi, S., Horth, J., Moortgat, G. K., R.Winterhalter, Myhre, C. E. L., Tsigaridis, K., Vignati, E., Stephanou, E. G., and J.Wilson: Organic aerosol and global climate modelling: a review, Atmos. Chem. Phys., 5, 1053-1123, 2005.

Lambe, A. T., Onasch, T. B., Croasdale, D. R., Wright, J. P., Martin, A. T., Franklin, J. P., Massoli, P., Kroll, J. H., Canagaratna, M. R., Brune, W. H., Worsnop, D. R., and Davidovits, P.: Transitions from functionalization to fragmentation reactions of laboratory secondary organic aerosol (SOA) generated from the OH oxidation of alkane precursors, Environ. Sci. Technol., 46, 5430-5437, 10.1021/es300274t, 2012.

Lamkaddam, H., Gratien, A., Ropion, M., Pangui, E., and Doussin, J. F.: Kinetic study of the temperature dependence of OH-initiated oxidation of n-dodecane, J. Phys. Chem. A, 123, 9462-9468, 10.1021/acs.jpca.9b07704, 2019.

Lamkaddam, H., Gratien, A., Pangui, E., David, M., Peinado, F., Polienor, J.-M., Jerome, M., Cazaunau, M., Gaimoz, C., Picquet-Varrault, B., Kourtchev, I., Kalberer, M., and Doussin, J.-F.: Role of relative humidity in the secondary organic aerosol formation from high-NOx photooxidation of long-chain alkanes: n-Dodecane case study, ACS Earth Space Chem., 4, 2414-2425, 10.1021/acsearthspacechem.0c00265, 2020.

Li, H., Zhang, Q., Zhang, Q., Chen, C., Wang, L., Wei, Z., Zhou, S., Parworth, C., Zheng, B., Canonaco, F., Prévôt, A. S. H., Chen, P., Zhang, H., Wallington, T. J., and He, K.: Wintertime aerosol chemistry and haze evolution in an extremely polluted city of the North China Plain: significant contribution from coal and biomass combustion, Atmos. Chem. Phys., 17, 4751-4768, 2017a.

Li, J., Li, K., Wang, W., Wang, J., Peng, C., and Ge, M.: Optical properties of secondary organic aerosols derived from long-chain alkanes under various NOx and seed conditions, Sci. Total Environ., 579, 1699-1705, 10.1016/j.scitotenv.2016.11.189, 2017b.

Li, J., Wang, W., Li, K., Zhang, W., Peng, C., Liu, M., Chen, Y., Zhou, L., Li, H., and Ge, M.: Effect of chemical structure on optical properties of secondary organic aerosols derived from C_{12} alkanes, Sci. Total Environ., 751, 141620, 10.1016/j.scitotenv.2020.141620, 2021a.

Li, J., Li, H., Li, K., Chen, Y., Zhang, H., Zhang, X., Wu, Z., Liu, Y., Wang, X., Wang, W., and Ge, M.: Enhanced secondary organic aerosol formation from the photo-oxidation of mixed anthropogenic volatile organic compounds, Atmos. Chem. Phys., 21, 7773-7789, 10.5194/acp-21-7773-2021, 2021b.

Li, J., Wang, W., Li, K., Zhang, W., Peng, C., Zhou, L., Shi, B., Chen, Y., Liu, M., Li, H., and Ge, M.: Temperature effects on optical properties and chemical composition of secondary organic aerosol derived from n-dodecane, Atmos. Chem. Phys. 20, 8123-8137, https://doi.org/10.5194/acp-20-8123-2020, 2020.

https://doi.org/10.5194/acp-2022-294
Preprint. Discussion started: 25 April 2022

Li, J., Li, H., Wang, X., Wang, W., Ge, M., Zhang, H., Zhang, X., Li, K., Chen, Y., Wu, Z., Chai, F., Meng, F., Mu, Y., Mellouki, A., Bi, F., Zhang, Y., Wu, L., and Liu，Yongchun: A Large-Scale Outdoor Atmospheric Simulation Smog Chamber for Studying Atmospheric Photochemical Processes: Characterization and Preliminary Application, J. Environ. Sci. 102, 185-197, 2021c.

Li, J., Li, K., Li, H., Wang, X., Wang, W., Wang, K., and Ge, M.: Long-chain alkanes in the atmosphere: A review, J. Environ. Sci., 10.1016/j.jes.2021.07.021, 2022.

Li, K., Liggio, J., Lee, P., Han, C., Liu, Q., and Li, S.-M.: Secondary organic aerosol formation from α-pinene, alkanes, and oil-sands-related precursors in a new oxidation flow reactor, Atmos. Chem. Phys., 19, 9715-9731, 10.5194/acp-19-9715-2019, 2019a.

Li, K., Liggio, J., Han, C., Liu, Q., Moussa, S. G., Lee, P., and Li, S. M.: Understanding the Impact of High-NOx Conditions on the Formation of Secondary Organic Aerosol in the Photooxidation of Oil Sand-Related Precursors, Environ. Sci. Technol., 53, 14420-14429, 10.1021/acs.est.9b05404, 2019b.

Li, K., Chen, L., White, S. J., Han, K., Lv, B., Bao, K., Wu, X., Gao, X., Azzi, M., and Cen, K.: Effect of nitrogen oxides (NO and NO_2) and toluene on SO_2 photooxidation, nucleation and growth: A smog chamber study, Atmos. Res., 192, 38-47, 10.1016/j.atmosres.2017.03.017, 2017c.

Li, K., Wentzell, J. J. B., Liu, Q., Leithead, A., Moussa, S. G., Wheeler, M. J., Han, C., Lee, P., Li, S.-M., and Liggio, J.: Evolution of atmospheric total organic carbon from petrochemical mixtures, Environ. Sci. Technol., 10.1021/acs.est.1c02620, 2021d.

Liggio, J. and Li, S. M.: A new source of oxygenated organic aerosol and oligomers, Atmos. Chem. Phys., 13, 2989-3002, 10.5194/acp-13-2989-2013, 2013.

Liu, C., Chen, T., Liu, Y., Liu, J., He, H., and Zhang, P.: Enhancement of secondary organic aerosol formation and its oxidation state by SO_2 during photooxidation of 2-methoxyphenol, Atmos. Chem. Phys., 19, 2687-2700, 10.5194/acp-19-2687-2019, 2019.

Liu, S., Jia, L., Xu, Y., Tsona, N. T., Ge, S., and Du, L.: Photooxidation of cyclohexene in the presence of SO_2: SOA yield and chemical composition, Atmos. Chem. Phys., 17, 13329-13343, 10.5194/acp-17-13329-2017, 2017.

Liu, T., Wang, X., Hu, Q., Deng, W., Zhang, Y., Ding, X., Fu, X., Bernard, F., Zhang, Z., Lü, S., He, Q., Bi, X., Chen, J., Sun, Y., Yu, J., Peng, P., Sheng, G., and Fu, J.: Formation of secondary aerosols from gasoline vehicle exhaust when mixing with SO_2, Atmos. Chem. Phys., 16, 675-689, 10.5194/acp-16-675-2016, 2016.

Loza, C. L., Craven, J. S., Yee, L. D., Coggon, M. M., Schwantes, R. H., Shiraiwa, M., Zhang, X., Schilling, K. A., Ng, N. L., Canagaratna, M. R., Ziemann, P. J., Flagan, R. C., and Seinfeld, J. H.: Secondary organic aerosol yields of 12-carbon alkanes, Atmos. Chem. Phys., 14, 1423-1439, 10.5194/acp-14-1423-2014, 2014.

Mao, J., Ren, X., Brune, W. H., Olson, J. R., Crawford, J. H., Fried, A., Huey, L. G., Cohen, R. C., Heikes, B., Singh, H. B., Blake, D. R., Sachse, G. W., Diskin, G. S., Hall, S. R., and Shetter, R. E.: Airborne measurement of OH reactivity during INTEX-B, Atmos. Chem. Phys., 9, 163-173, 2009.

Ming, L., Jin, L., Li, J., Fu, P., Yang, W., Liu, D., Zhang, G., Wang, Z., and Li, X.: $PM_{2.5}$ in the Yangtze River Delta, China: Chemical compositions, seasonal variations, and regional pollution events, Environ. Pollut., 223, 200-212, 10.1016/j.envpol.2017.01.013, 2017.

Nakayama, T., Sato, K., Imamura, T., and Matsumi, Y.: Effect of Oxidation Process on Complex Refractive Index of Secondary Organic Aerosol Generated from Isoprene, Environ. Sci. Technol., 52, 2566-2574, 10.1021/acs.est.7b05852, 2018.

Nakayama, T., Sato, K., Tsuge, M., Imamura, T., and Matsumi, Y.: Complex refractive index of secondary organic aerosol generated from isoprene/NOx photooxidation in the presence and absence of SO_2, J. Geophys. Res. Atmos., 120, 7777-7787, 10.1002/2015jd023522, 2015.

Ng, N. L., Kroll, J. H., Chan, A. W. H., Chhabra, P. S., Flagan, R. C., and Seinfeld, J. H.: Secondary organic aerosol formation from m-xylene, toluene, and benzene, Atmos. Chem. Phys., 7, 3909-3922, 2007.

Qi, L., Liu, H., Shen, X., Fu, M., Huang, F., Man, H., Deng, F., Shaikh, A. A., Wang, X., Dong, R., Song, C., and He, K.: Intermediate-volatility organic compound emissions from nonroad construction machinery under different operation modes, Environ. Sci. Technol., 53, 13832-13840, 10.1021/acs.est.9b01316, 2019.

Qi, L., Zhao, J., Li, Q., Su, S., Lai, Y., Deng, F., Man, H., Wang, X., Shen, X., Lin, Y., Ding, Y., and Liu, H.: Primary organic gas emissions from gasoline vehicles in China: Factors, composition and trends, Environ. Pollut., 290, 117984, 10.1016/j.envpol.2021.117984, 2021.

Requia, W. J., Higgins, C. D., Adams, M. D., Mohamed, M., and Koutrakis, P.: The health impacts of weekday traffic: A health risk assessment of $PM_{2.5}$ emissions during congested periods, Environ. Int., 111, 164-176, 10.1016/j.envint.2017.11.025, 2018.

S. Guo, M. Hu, Z. B. Wang, J. Slanina, and Zhao, Y. L.: Size-resolved aerosol water-soluble ionic compositions in the summer of Beijing: implication of regional secondary formation, Atmos. Chem. Phys., 10, 947-959, 2010.

Santiago, M., Vivanco, M. G., and Stein, A. F.: SO2 effect on secondary organic aerosol from a mixture of anthropogenic VOCs: experimental and modelled results, International J. Environ. Pollut., 50, 224, 10.1504/ijep.2012.051195, 2012.

Sheehan, P. E. and Bowman, F. M.: Estimated effects of temperature on secondary organic aerosol concentrations, Environ. Sci. Technol., 35, 10.1021/es001547g, 2001.

Shi, B., Wang, W., Zhou, L., Li, J., Wang, J., Chen, Y., Zhang, W., and Ge, M.: Kinetics and mechanisms of the gas-phase reactions of OH radicals with three C15 alkanes, Atmos. Environ., 207, 75-81, 10.1016/j.atmosenv.2019.03.028, 2019a.

Shi, B., Wang, W., Zhou, L., Sun, Z., Fan, C., Chen, Y., Zhang, W., Qiao, Y., Qiao, Y., and Ge, M.: Atmospheric oxidation of C10~14 n-alkanes initiated by Cl atoms: Kinetics and mechanism, Atmos. Environ., 222, 117166, 10.1016/j.atmosenv.2019.117166, 2019b.

Sipila, M., Berndt, T., Petaja, T., Brus, D., Vanhanen, J., Stratmann, F., Patokoski, J., Mauldin, R. L., Hyvarinen, A. P., Lihavainen, H., and Kulmala, M.: The role of sulfuric acid in atmospheric nucleation, Science, 327, 1243-1246, 10.1126/science.1180315, 2010.

Sivaramakrishnan, R. and Michael, J. V.: Rate constants for OH with selected large alkanes: Shock-tube measurements and an improved group scheme, J. Phys. Chem. A, 113, 5047-5060, 10.1021/jp810987u, 2009.

Tadeusz E. Kleindienst, Edney, E. O., LewandowskiI, M., Offenberg, J. H., and Jaoui, M.: Secondary organic carbon and aerosol yields from the irradiations of isoprene and r-pinene in the presence of NO_x and SO_2, Environ. Sci. Technol., 40, 3807-3812, 2006.

Takekawa, H., Minoura, H., and Yamazaki, S.: Temperature dependence of secondary organic aerosol formation by photo-oxidation of hydrocarbons, Atmos. Environ., 37, 3413-3424, 10.1016/s1352-2310(03)00359-5, 2003.

Tsai, S. S., Chang, C. C., and Yang, C. Y.: Fine particulate air pollution and hospital admissions for chronic obstructive pulmonary disease: a case-crossover study in Taipei, Int. J. Environ. Res. Pub. He., 10, 6015-6026, 10.3390/ijerph10116015, 2013.

Tsiligiannis, E., Hammes, J., Salvador, C. M., Mentel, T. F., and Hallquist, M.: Effect of NOx on 1,3,5-trimethylbenzene (TMB) oxidation product distribution and particle formation, Atmos. Chem. Phys., 19, 15073-15086, 10.5194/acp-19-15073-2019, 2019.

Wall, K. J. and Harris, G. W.: Uptake of nitrogen dioxide (NO_2) on acidic aqueous humic acid (HA) solutions as a missing daytime nitrous acid (HONO) surface source, J. Atmos. Chem., 74, 283-321, 10.1007/s10874-016-9342-8, 2016.

Wang, C., Yuan, B., Wu, C., Wang, S., Qi, J., Wang, B., Wang, Z., Hu, W., Chen, W., Ye, C., Wang, W., Sun, Y., Wang, C., Huang, S., Song, W., Wang, X., Yang, S., Zhang, S., Xu, W., Ma, N., Zhang, Z., Jiang, B., Su, H., Cheng, Y., Wang, X., and Shao, M.: Measurements of higher alkanes using NO+ chemical ionization in PTR-ToF-MS: important contributions of higher alkanes to secondary organic aerosols in China, Atmos. Chem. Phys., 20, 14123-14138, 10.5194/acp-20-14123-2020, 2020a.

Wang, S., Du, L., Tsona, N. T., Jiang, X., You, B., Xu, L., Yang, Z., and Wang, W.: Effect of NOx and SO_2 on the photooxidation of methylglyoxal: Implications in secondary aerosol formation, J. Environ. Sci. (China), 92, 151-162, 10.1016/j.jes.2020.02.011, 2020b.

Wang, W. G., Liu, M. Y., Wang, T. T., Song, Y., Zhou, L., Cao, J. J., Hu, J. N., Tang, G. G., Chen, Z., Li, Z. J., Xu, Z. Y., Peng, C., Lian, C. F., Chen, Y., Pan, Y. P., Zhang, Y. H., Sun, Y. L., Li, W. J., Zhu, T., Tian, H. Z., and Ge, M. F.: Sulfate formation is dominated by manganese-catalyzed oxidation of SO2 on aerosol surfaces during haze events, Nat. Commun., 12, 10, 10.1038/s41467-021-22091-6, 2021.

Wang, Y., Wang, Y., Wang, L., Petäjä, T., Zha, Q., Gong, C., Li, S., Pan, Y., Hu, B., Xin, J., and Kulmala, M.: Increased inorganic aerosol fraction contributes to air pollution and haze in China, Atmos. Chem. Phys., 19, 5881-5888, 10.5194/acp-19-5881-2019, 2019.

Warren, B., Austin, R. L., and Cocker, D. R.: Temperature dependence of secondary organic aerosol, Atmos. Environ., 43, 3548-3555, 10.1016/j.atmosenv.2009.04.011, 2009.

Wu, L. Y., Tong, S. R., Zhou, L., Wang, W. G., and Ge, M. F.: Synergistic effects between SO_2 and HCOOH on alpha-Fe2O3, J. Phys. Chem. A, 117, 3972-3979, 10.1021/jp400195f, 2013.

https://doi.org/10.5194/acp-2022-294
Preprint. Discussion started: 25 April 2022

Atmospheric Chemistry and Physics Discussions

Xu, R., Alam, M. S., Stark, C., and Harrison, R. M.: Composition and emission factors of traffic- emitted intermediate volatility and semi-volatile hydrocarbons (C_{10}–C_{36}) at a street canyon and urban background sites in central London, UK, Atmos. Environ., 231, 117448, 10.1016/j.atmosenv.2020.117448, 2020.

Yang, Z., Tsona, N. T., Li, J., Wang, S., Xu, L., You, B., and Du, L.: Effects of NOx and SO_2 on the secondary organic aerosol formation from the photooxidation of 1,3,5-trimethylbenzene: A new source of organosulfates, Environmental pollution, 264, 114742, 10.1016/j.envpol.2020.114742, 2020.

Zhang, Q., Zheng, Y., Tong, D., Shao, M., Wang, S., Zhang, Y., Xu, X., Wang, J., He, H., Liu, W., Ding, Y., Lei, Y., Li, J., Wang, Z., Zhang, X., Wang, Y., Cheng, J., Liu, Y., Shi, Q., Yan, L., Geng, G., Hong, C., Li, M., Liu, F., Zheng, B., Cao, J., Ding, A., Gao, J., Fu, Q., Huo, J., Liu, B., Liu, Z., Yang, F., He, K., and Hao, J.: Drivers of improved PM2.5 air quality in China from 2013 to 2017, Proc. Natl. Acad. Sci. USA, 116, 24463-24469, 10.1073/pnas.1907956116, 2019.

Zhang, W., Wang, W., Li, J., Peng, C., Li, K., Zhou, L., Shi, B., Chen, Y., Liu, M., and Ge, M.: Effects of SO_2 on optical properties of secondary organic aerosol generated from photooxidation of toluene under different relative humidity, Atmos. Chem. Phys. 20, 4477–4492, 10.5194/acp-20-4477-2020, 2020.

Zhang, X., Cappa, C. D., Jathar, S. H., McVay, R. C., Ensberg, J. J., Kleeman, M. J., and Seinfeld, J. H.: Influence of vapor wall loss in laboratory chambers on yields of secondary organic aerosol, P. Natl. Acad. Sci. USA 111, 5802-5807, 2014.